Chemical Physics 84 (1984) 51–60
North-Holland, Amsterdam

INTERSYSTEM CROSSING FROM SINGLET STATES OF MOLECULAR DIMERS AND MONOMERS IN MIXED MOLECULAR CRYSTALS: PICOSECOND STIMULATED PHOTON ECHO EXPERIMENTS

F.G. PATTERSON, H.W.H. LEE, William L. WILSON and M.D. FAYER

Department of Chemistry, Stanford University, Stanford, California 94305, USA

Received 7 September 1983

An experimental study of the excited-state dynamics of pentacene dimers and monomers in *p*-terphenyl host crystals is presented. Picosecond stimulated photon echoes, picosecond photon echoes, and fluorescence lifetime measurements are used to study intersystem crossing and homogeneous dephasing of delocalized dimers and monomers at 1.8 K. It is found that the dimer states can have intersystem crossing rate constants which are orders of magnitude greater than the corresponding monomers. Three mechanisms are considered to explain the differences between dimer and monomer intersystem crossing. Fluorescence lifetime measurements and photon echo measurements demonstrate that the only source of homogeneous line broadening at 1.8 K is population relaxation. These measurements combined with the stimulated echo measurements show that differences in lifetimes exhibited by the various dimer and various monomer sites are due solely to differences in intersystem crossing rate constants.

1. Introduction

Molecular pairs or dimers appear as important components in diverse range of problems [1–4]. For example, the triplet states of chlorophyll dimers are involved in the photosynthetic process [1]. In molecular crystals, nearest-neighbor substitutional dimers of molecules such as pentacene [2], tetrachlorobenzene [3], and naphthalene [4,5], have been studied as the simplest systems capable of showing delocalization of an electronic excitation over more than one molecule. Dimer triplet states, [3,4] and singlet states [2,5] have been studied with the principal interest being the coherence time associated with the delocalized state.

In this paper we present picosecond time scale optical coherence experiments, particularly stimulated photon echo experiments, which are used to examine intersystem crossing (ISC) in nearest-neighbor substitutional dimers of pentacene in *p*-terphenyl host crystals at 1.8 K. A number of different pair states are examined and contrasted to the results obtained from experiments on pentacene monomers in the four different sites [6,7] in the *p*-terphenyl host crystal.

In the sixties and early seventies basic factors controlling spin–orbit coupling (SOC) and therefore ISC in isolated molecules were elucidated [8]. Ratios of ISC rates to the three spin sublevels of T_1, the first triplet state, from the first singlet state, S_1, were determined in some mixed-crystal systems [9]. Lifetimes, and relative populations of the spin sublevels were also measured [9] at ≈ 4.2 K. The experiments involved both phosphorescence and electron paramagnetic resonance methods, in particular, optically detected magnetic resonance techniques. However, these experiments are incapable of determining the absolute rate of ISC from S_1 to T_1.

ISC, along with internal conversion and radiative decay are the three fundamental processes which govern the lifetime of S_1. SOC is a relatively weak effect for organic molecules. In particular, for $\pi\pi^*$ transitions of planar aromatic hydrocarbons such as pentacene, SOC between the S_1 and T_1 states having the same symmetry spatial wavefunctions is forbidden by symmetry [10].

Therefore ISC is expected to be very slow and not to significantly influence the S_1 lifetime. However a variety of factors, such as vibronic coupling [9] or a second triplet state [11] close to S_1 in energy can dramatically affect ISC rates resulting in a significant T_1 yield and shortening of the S_1 lifetime.

Recently Morsink et al. [12] applied picosecond stimulated photon echo experiments (a three-pulse echo sequence used extensively in magnetic resonance [13]) to directly measure the ISC rate and yield for pentacene in naphthalene at 1.8 K. Earlier, other optical coherence methods were used to qualitatively examine ISC in pentacene monomers in the four sites of *p*-terphenyl. [14,15].

The *p*-terphenyl host crystal has four inequivalent molecules in the unit cell [6]. The four unit cell positions differ by the twist angle of the *p*-terphenyl rings away from planarity. The environment of a pentacene replacing a *p*-terphenyl molecule will be different in each of the four positions. This difference manifests itself as four $S_0 \rightarrow S_1$ pentacene origins in the absorption spectrum [7]. These are referred to as O_1 through O_4. O_1 is the line farthest to the red. O_1 and O_2 have a splitting of only $\approx 4\ cm^{-1}$ while the O_1–O_3 and O_1–O_4 splitting are $\approx 123\ cm^{-1}$ and $\approx 182\ cm^{-1}$, respectively.

Measurements of ISC rates, homogeneous dephasing times and lifetimes for the four pentacene monomer origins provide a useful context for understanding these same experiments performed on delocalized dimer states. The O_1 and O_2 origins have S_1 lifetimes which are greater than twice as long as the O_3 and O_4 lifetimes. Williams et al. [11] have performed temperature-dependent lifetime measurements on these four lines. Observing a temperature-dependent lifetime for O_1 and O_2 but not for O_3 and O_4, they postulated that the lifetime shortening in O_3 and O_4 was due to greatly increased ISC to an accessible second triplet, T_2. However, other workers have reported the absence of a temperature dependence to the O_1 and O_2 lifetimes [14]. In this paper we report the low-temperature lifetimes, τ_f, homogeneous dephasing times, T_2, ISC rate constants, k_{23}, and the ISC yields for O_1 through O_4. These results demonstrate that the difference between the lifetimes is due solely to differences in the ISC rate constants. We also confirm the temperature dependence of the O_1 and O_2 lifetimes. These results reinforce the previously postulated mechanism for the differences in ISC [11].

We then examine the three well-resolved dimer states labeled R_3, R_4 and R_5 which are built off of the O_1 and O_2 origins and are shifted to the red of O_1. These delocalized dimer states arise from the various nearest-neighbor geometries of pentacene pairs in the *p*-terphenyl host crystal. Again we report the low-temperature lifetimes, homogeneous dephasing times, ISC rate constants, and the ISC yields of each of the dimer states. Although the monomers O_1 and O_2 have virtually no ISC, we observe that R_5 and R_4 have a great deal of ISC while R_3 has considerably less. *Thus dimers can have substantially different intersystem crossing rate constants than the constituent monomers, and dimers with different spatial configurations can have wide variations in intersystem crossing although they are composed of the same monomers.*

Three possible mechanisms to explain the differences between monomers and dimers and between different dimers are suggested and discussed. The first is a mechanical distortion of the pentacene molecule upon dimer formation which results in a reduction in the molecular symmetry and therefore a change in SOC paths and ISC. The second involves intermolecular SOC terms which can arise for delocalized states [10]. These intermolecular terms open up additional SOC routes and can increase ISC. Intermolecular spin–orbit interactions have been proposed to explain SOC differences between a triplet exciton and the corresponding isolated molecule [10]. The third possible mechanism is the same as that proposed to explain the differences between O_1, O_2 monomers and O_3, O_4 monomers, i.e. small changes in the electronic wavefunctions can shift a second nearby triplet, T_2, above or below S_1 in energy. For those states in which T_2 is below S_1 (presumably O_3, O_4, R_4 and R_5) ISC is fast, while for the other states (O_1, O_2 and R_3) for which T_2 is above S_1 ISC is slow. While it is not possible to decide definitively between these three mechanisms, it is suggested that the third mechanism is most plausible.

2. Experimental procedures

The picosecond light pulses were provided by a mode-locked, cavity-dumped dye laser synchronously pumped by the frequency-doubled output of a cw-pumped acousto-optically mode-locked and Q-switched Nd:YAG laser [16]. This dye laser provides a stable source of tunable 30 ps, 20 μJ pulse at an 800 Hz repetition rate.

In the photon echo (PE) and stimulated echo (SE) experiments, a dye laser single pulse is split into two or three excitation pulses of appropriate energies [2]. In both the PE and SE experiments one pulse is directed into a corner cube on a motorized multipass delay line to provide a 0 to 36 ns variable temporal delay between the excitation pulses. In the three-pulse SE experiment, the time separation between the first two pulses is fixed at 2 ns while the separation between the second and third pulses was varied from 0 to 36 ns.

Non-collinear excitation geometry was employed to spatially isolate the echo signals. In the PE experiments, the angle between the two excitation beams was 2.5°, while in the SE experiments the angle between the first and second excitation beams was 1.25° and the angle between the second and third was 2.25°. In order to enhance detection sensitivity in the PE and SE experiments, the excitation beam located spatially farthest from the echo signal was chopped at one-half the repetition rate of the laser. The echo signals were directed into a dry-ice-cooled photomultiplier tube (PMT), and detected with a lock-in amplifier at one-half the laser repetition rate. When the delay line is run, the output of the lock-in amplifier and a voltage proportional to the temporal delay are digitized and stored on disk for subsequent analysis.

It has been demonstrated that for samples with finite optical density (OD ≥ 0.05), a power-dependent optical pulse shaping effect contributes to the echo decay if the decay occurs on the same time scale as the excited-state lifetime [17]. Therefore a careful study of the decay versus power was performed for each spectral line of each sample to ensure that the decay reflected only intrinsic molecular properties.

In the fluorescence lifetime measurements, the dye laser single pulse which is cavity-dumped by a Pockels cell was passed through a second Pockels cell and cube polarizer to completely eliminate the very small leakage pulses which normally follow the dye laser single pulse. The pulse was then passed through a Spex $\frac{1}{4}$ m monochromator to filter out any unwanted laser frequencies and cavity fluorescence. Fluorescence decays were obtained by detecting at right angles with a Hamamatsu R1645 u-01 microchannel plate PMT and a computer-interfaced Tektronix R-7912 transient digitizer. A 647.1 nm interference filter (Ealing) and five 600 nm sharp cut long-pass filters (Hoya) were fitted over the PMT. This particular set of filters was chosen because the filters themselves did not fluoresce while many other filters were found to produce considerable fluorescence. They pass the most intense fluorescence lines of the pentacene in p-terphenyl mixed-crystal system, and they blocked all other extraneous fluorescence, e.g., fluorescence originating from the dewar windows. Inaccuracies in the lifetime measurement arising from re-absorption of fluorescence by the sample were avoided by using data only from those samples which were deemed to have sufficiently low optical density. It was found that samples with even a few percent absorption were not usable and only samples with $< 0.5\%$ absorption give consistent results independent of sample.

The pentacene in p-terphenyl mixed crystals were grown by the Bridgman technique using extensively zone-refined p-terphenyl. The pentacene obtained from Aldrich was vacuum sublimed once before use. The S_0 to S_1 pentacene transition in p-terphenyl is strongly b-axis polarized [18]. The crystals were cleaved along the ab plane and a conoscopic microscope with crossed polarizers was used to locate the optic axis to ensure that the crystal b axis was parallel to the laser polarization.

3. Results and discussion

3.1. Pentacene monomer intersystem crossing

Pentacene in the low-temperature p-terphenyl lattice exhibits four distinct sites (fig. 1). These sites result from the p-terphenyl phase transition

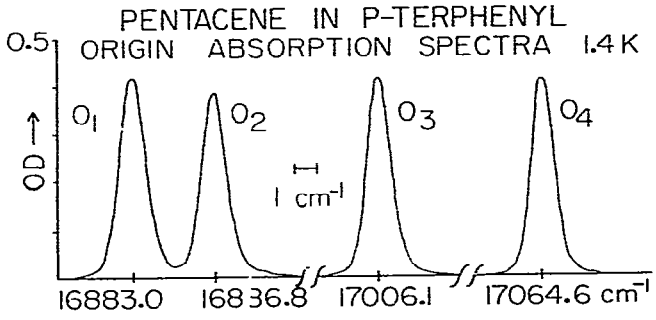

Fig. 1. Typical pentacene in *p*-terphenyl transmission spectra at 1.4 K of the four $S_0 \rightarrow S_1$ origins, O_1–O_4. Note that they are virtually identical in shape, width, and height. Pentacene is 3×10^{-6} mol/mole.

at ≈ 190 K in which *p*-terphenyl ring rocking freezes out [6]. The final ring distribution produces a low-temperature unit cell which contains four conformationally different *p*-terphenyl molecules. According to fully relaxed atom–atom potential calculations [19], each pentacene molecule replaces one *p*-terphenyl molecule in the lattice substitutionally yielding four conformationally different pentacene environments. Since the crystals are grown well above the phase-transition temperature, pentacenes populate the four sites equally (see fig. 1).

The low-temperature fluorescence lifetimes and PE and SE results for the four monomer origins are given in table 1. Note that at low temperature T_2 is determined solely by the fluorescence lifetime, i.e. $T_2 = 2\tau_f$ (fig. 2). The only source of homogeneous line broadening is population relaxation; there is no pure dephasing at this temperature [☆]. Also, note the substantial decrease in the fluorescence lifetime for the O_3 and O_4 sites compared to the O_1 and O_2 sites. It has been shown that the fluorescence lifetimes for O_1 and O_2 are faster than expected from radiative contributions alone [14]. The lifetime reduction is attributed to a 22% yield for S_1 to S_0 internal conversion. However, because of a large uncertainty in measuring the ISC rates for O_3 and O_4, this same study was unable to determine whether the further reduction in the fluorescence lifetimes for O_3 and O_4 is due to a greater degree of internal conversion or a substantial increase in ISC, or both. From the results of SE experiments given below, we show that the O_3, O_4 lifetime reductions are due exclusively to an increase in ISC.

In the SE experiment O_1 and O_2 exhibited exponential decays with time constants given by their fluorescence lifetimes, i.e. $k_f^{SE} = 1/\tau_f$. (Fig. 3 illustrates an exponential SE decay with data from the R_3 line discussed below. O_1 and O_2 data have the same appearance.) The fact that the O_1, O_2 decays are pure exponentials on the time scale of measurement is consistent with previous reports of extremely low ISC yields ($< 0.5\%$) for the origins [14]. The SE decays of O_3 and O_4 are markedly different: highly non-exponential with long-lived tails (see fig. 4 and inset). To interpret this non-exponential SE data we use the following expression

☆ The previously reported [2,17,20] small difference between T_2 and $2\tau_f$ at this temperature was caused by a small amount of fluorescence reabsorption, lengthening the measured lifetime, τ_f.

Table 1
Rate constants and ISC yields for pentacene monomers (all rate constants have been multiplied by 10^{-7})

Monomer	$1/\tau_f$	$2/T_2$	k_f^{SE} [a]	k_{21}	k_{23}	ISC yield (β)
O_1	4.6±0.2	4.9±0.4	4.7±0.2	–	–	0.0047±0.001 [b]
O_2	4.4±0.3	4.6±0.3	4.3±0.2	–	–	0.0038±0.001 [b]
O_3	10.8±0.6	11.4±0.8	11.8±0.4	4.2±0.3	7.5±0.5	0.64 ±0.02
O_4	10.6±0.7	11.6±1.0	11.5±0.2	4.5±0.2	7.0±0.5	0.61 ±0.02

[a] k_f^{SE} is the total S_1 population decay constant determined by the SE. $k_f^{SE} = k_{21} + k_{23}$. When $k_{23} = 0$, the SE decay is exponential. k_f^{SE} in all cases should equal $1/\tau_f$ measured by fluorescence decay.

[b] See ref. [14].

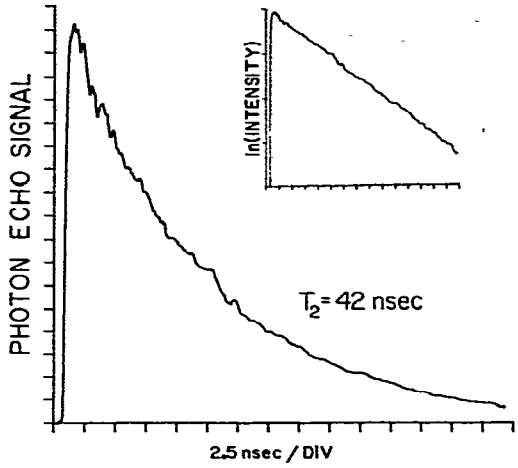

Fig. 2. Photon echo decay of the O_2 site of pentacene in *p*-terphenyl at 1.8 K. The exponential decay (see inset) gives a $T_2 = 42$ ns ($I_{PE} = I_0 \exp(-4t/T_2)$). This demonstrates $T_2 = 2\tau_f$, i.e. the only source of homogeneous line broadening is population relaxation.

given by Morsink et al. [12] for a three-level system in which level 3 is a bottleneck state not coupled to the radiation field:

$$I_{SE} = I_0[(2-\beta)\exp(-t/\tau_f) + \beta\exp(-k_{31}t)]^2, \quad (1)$$

where $\beta = k_{23}/(k_{21} + k_{23} - k_{31})$ and $1/\tau_f = k_{21} + k_{23}$. The rate constants are as pictured in fig. 5.

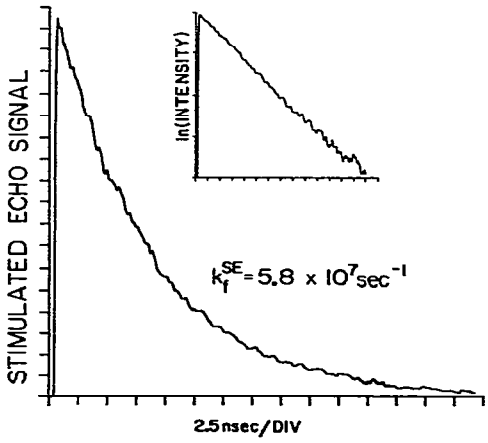

Fig. 3. An example of an exponential stimulated echo decay. The data was taken on the R_3 dimer line at 1.8 K. The inset gives the log of the data which is exponential on the time scale of these experiments. This indicates a slow ISC rate. k_f^{SE}, the decay constant, equals $1/\tau_f$.

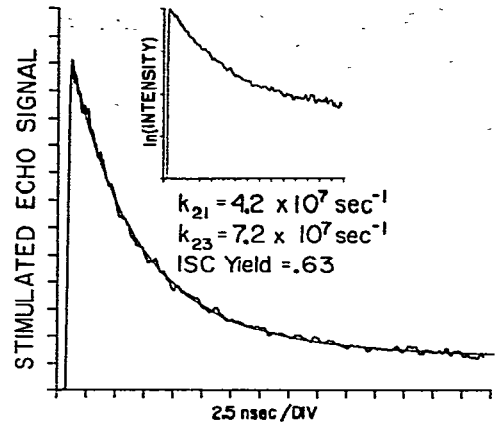

Fig. 4. An example of a non-exponential stimulated echo decay. The data was taken on the O_3 monomer line at 1.8 K. The decay is highly non-exponential, indicating a fast ISC rate (ISC yield = 0.63). The solid line through the data is the best fit to the data giving the constants k_{23} and k_{21}. k_{23} is the ISC rate constant and k_{21} is the S_1 to S_0 decay constant.

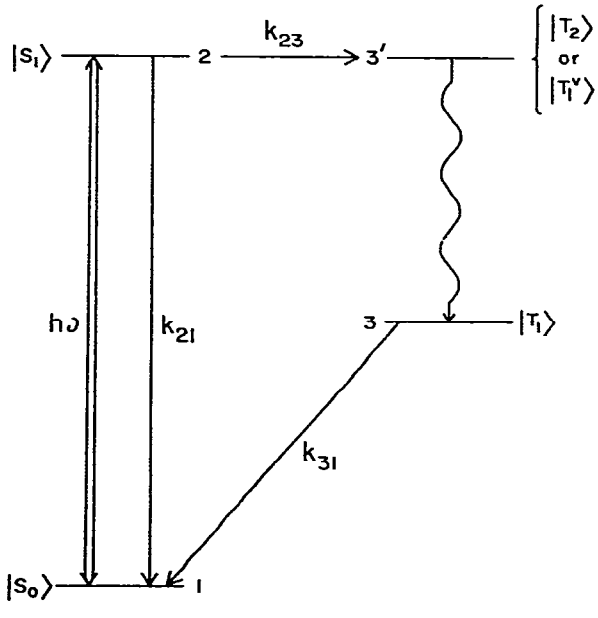

Fig. 5. Energy level diagram illustrating the basic scheme for both monomers and dimers. The double headed arrow represents the coupling by the radiation field. The initially populated triplet level, 3', is either a high lying vibration of T_1, $|T_1^v\rangle$, or the second triplet state, $|T_2\rangle$. The wavy arrow connecting 3' with the vibrationally unexcited first triplet, 3, represents rapid radiationless relaxation which does not contribute to the time dependence of the experiments. k_{23} is the ISC rate constant. k_{21} is the rate constant for S_1 to S_0 population decay.

This energy-level diagram illustrates the basic scheme for both monomers and dimers. The double headed arrow represents coupling of the levels by the radiation field. The initially populated triplet level, 3', is either a high-lying vibration of T_1, $|T_1'\rangle$, or the second triplet state, $|T_2\rangle$. The wavy arrow connecting 3' with the vibrationally unexcited first triplet, 3, represents rapid radiationless relaxation which does not contribute to the time dependence of the experiments. k_{23} is the ISC rate constant. k_{21} is the rate constant for S_1 to S_0 population decay. τ_f is the fluorescence lifetime for the S_1 excited state and $1/k_{31}$ is the triplet lifetime. This equation treats the triplet state as a single level which is valid when the lifetimes of the three-spin sublevels are all long compared to the time scale of the experiment and the repetition time of the experiment (≈ 1 ms) is slow compared to the triplet lifetimes (10–100 μs) [14].

Although eq. (1) contains the triplet lifetime, $1/k_{31}$, the analysis of the experimental data to obtain information on the singlet dynamics is independent of k_{31}. k_{31} is on the order of 10^4–10^5 s^{-1} [14] while the time scale of the experiment is 10^{-8} s. Thus the second exponential in eq. (1) will remain constant, and since k_{21} and k_{23} are of order 10^8 s^{-1}, the value of β is just $k_{23}/(k_{21}+k_{23})$, the intersystem crossing yield. In addition, $k_{21}+k_{23}=1/\tau_f$. This gives an additional test on the values obtained for k_{21} and k_{23} which can be determined accurately. A non-linear least-squares analysis using a modified algorithm due to Bevington [21] was employed to fit the non-exponential SE data. k_{21} and k_{23} were allowed to vary while $1/k_{31}$ was held fixed at 45 μs [14]. Since the noise on the data results in a small uncertainty in I_0, several values of I_0 in a small range were tried, with little effect on the results. Several different initial guesses were tried for each data set, all yielding the same results. SE data for O_3 is shown in fig. 4 along with a fit to the data. The results of such fits from a number of data sets on several crystals were used to obtain the rate constants and ISC yields presented in table 1. Note the good agreement between the rate constants obtained from fluorescence decay measurements ($1/\tau_f$) and those from fitting the non-exponential SE data ($k_f^{SE}=k_{21}+k_{23}$). Also, returning to a point made earlier, k_{21} for O_3 and O_4 is very nearly identical to $1/\tau_f$ measured for O_1 and O_2 demonstrating that the faster fluorescence decays observed for O_3 and O_4 are due to increased ISC.

As mentioned in section 1, Williams [11] proposed that the lifetime differences were due to the location of the second triplet state, T_2, of pentacene. It was suggested that pentacene in O_3, O_4 sites has T_2 somewhat below S_1, while pentacene in O_1, O_2 sites has T_2 somewhat above S_1. If T_2 has a different symmetry than T_1, then the symmetry restrictions that inhibit spin–orbit coupling between S_1 and T_1 may not apply to coupling between S_1 and T_2, permitting rapid intersystem crossing to T_2 followed by radiationless relaxation to T_1. At low temperature, this pathway is thermally inaccessible to O_1 and O_2, but evidently becomes accessible as the temperature is increased (see fig. 6). In fig. 6, the circles are the data of Williams [11] giving the O_1, O_2 lifetimes as a function of temperature. Other workers reported no temperature dependence [14]. The squares with error bars in fig. 6 are lifetime measurements made in this study, confirming the temperature dependence. Thermal activation makes T_2 accessible to

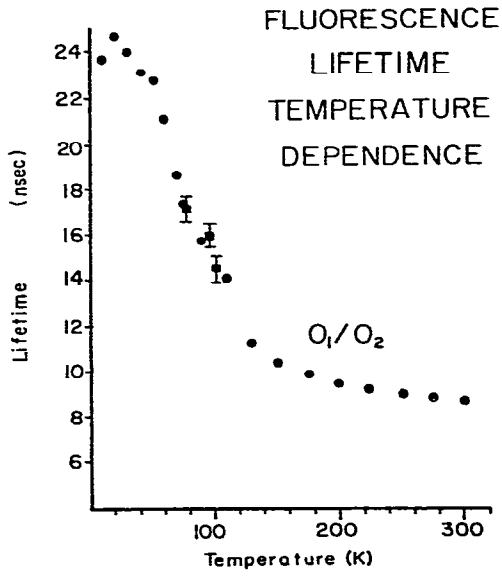

Fig. 6. Temperature dependence of the O_1, O_2 monomer origins. Solid circles are data from Williams et al. [11]. Solid squares with error bars are data from this study.

O_1, O_2, increasing ISC and decreasing the singlet lifetime. The temperature dependence suggests that T_2 is a few tens of cm^{-1} above S_1 for O_1, O_2. We also confirm the absence of temperature dependent lifetimes for O_3, O_4 which is consistent with the postulate that T_2 is below S_1 for these sites and that O_3, O_4 do not exhibit thermally activated increases in ISC.

3.2. Dimer intersystem crossing

Fig. 7 shows a transmission of a high concentration crystal of pentacene in *p*-terphenyl in the vicinity of the $S_0 \rightarrow S_1$ absorption origins, O_1 and O_2, of pentacene monomers [2]. The O_1 and O_2 origins coalesce into a broad and flat-topped peak because of the very high monomer concentration resulting in zero transmittance in the vicinity of the monomer origins. To the red of the broad origins lie three well-resolved peaks labeled R_3, R_4, and R_5, which have previously been shown to arise from pentacene dimer states [2]. Several other less-resolved peaks, labeled R_1 and R_2, can also be observed on the side of the monomer absorption, and using a form of optical T_2 selective photon echo excitation spectroscopy [2], several dimer states can be identified in the phonon side band to the blue of the O_1, O_2 origins. We will focus our attention on R_3, R_4, and R_5 since they are well resolved. Dimer states to the blue of O_1, O_2 and dimer states split off of O_3 and O_4 are obscured by the intense phonon sidebands of the origins. Although it is possible to perform optical coherence measurements on states buried beneath the sidebands [2], it is not possible to make fluorescence lifetime measurements directly.

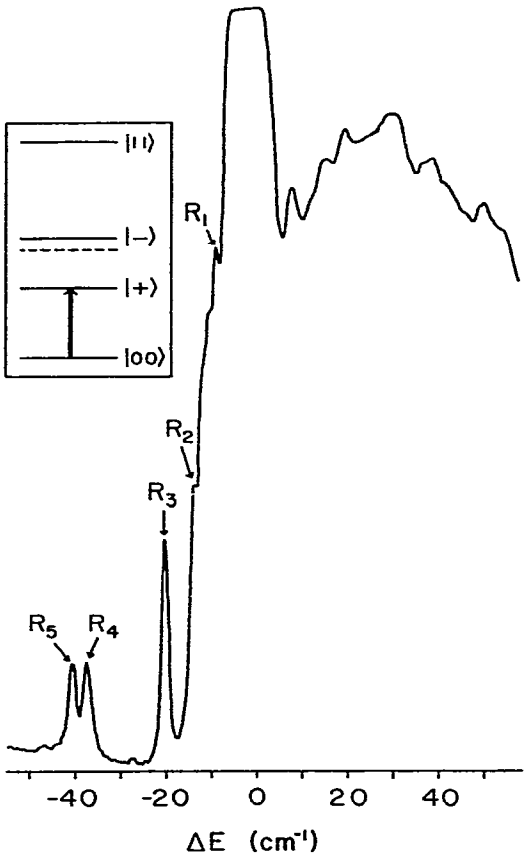

Fig. 7. Transmission spectrum in the region about the pentacene in *p*-terphenyl $S_0 \rightarrow S_1$ monomer O_1, O_2 origins at 1.4 K. The high pentacene concentration results in a broad flat monomer peak. The zero of energy is taken between the monomer O_1 and O_2 site origins. Five pentacene dimer peaks are labeled R_1 through R_5. The inset illustrates a dimer level scheme in which the dashed line represents the monomer energy. The dimer absorptions are shifted from the monomer absorptions, see text.

The three dimer states R_3, R_4, and R_5 are built off of the O_1, O_2 origins. These states are the delocalized excitations of pairs of pentacenes; the two pentacenes are both in O_1 sites, both in O_2 sites or one in an O_1 site and one in an O_2 site. Fully relaxed atom–atom potential calculations [19] demonstrate that pentacene monomers go into the crystal lattice with an orientation nearly identical to that of the *p*-terphenyl it replaces. Furthermore, this substitution produces very little structural disturbance in the surrounding host crystal [19]. Therefore, substituting in a second pentacene molecule at a site neighboring a pentacene will not disrupt the nearby *p*-terphenyl crystal structure, and the identity of the sites will be preserved. The observed energy splittings for dimers both to the red and blue of the O_1 and O_2 origins are consistent with those predicted by dipole–dipole calculations which assume that the two molecules in the dimer pair go into O_1, O_2 sites substitutionally for the *p*-terphenyl molecules [2].

The results of extensive temperature-dependent measurements [2] on R_3, R_4 and R_5 demonstrate that scattering between associated pairs of dimer levels does not occur to any significant extent at

the temperature of these experiments (1.8 K). Therefore, when a particular dimer level is selected by tuning the laser to the appropriate frequency, the population kinetics of that level is independent of the existence of its delocalized partner state. The system can then be considered in terms of the energy level diagram, fig. 5. Level 1 is the S_0 ground state of the dimer. Level 2 is a dimer delocalized state (see inset fig. 7). Level 3 is the triplet manifold of the dimer. The state T_1 is now a pair of triplet dimer states, each with three spin sublevels. As with the monomers, it is sufficient to consider T_1 as represented by a single level, since the triplet state relaxation rates do not enter into the interpretation of the experimental data.

The low-temperature fluorescence lifetimes, PE and SE results for the R_3, R_4 and R_5 dimer states are given in table 2. As in the case of the monomers, note that $T_2 = 2\tau_f$, demonstrating that the only source of homogeneous line broadening is excited-state relaxation. The SE decay for R_3 is purely exponential (see fig. 3), and decays with a rate constant $k_f^{SE} = 1/\tau_f$. Except for a small change in lifetime, this is the same as the O_1 and O_2 behavior. However, the stimulated echo decay of R_5 is highly non-exponential and the decay of R_4 is moderately non-exponential. The R_4 and R_5 SE decays were fit with the same equation and procedure used above on the O_3 and O_4 non-exponential data. The fits to the data are excellent with the same appearance as displayed in fig. 4.

Parameters listed in table 2 were obtained by averaging the results of a number of data sets on several crystals. Again there is good agreement between the lifetimes obtained from fluorescence decay measurements and those obtained from fitting the non-exponential stimulated echo data, confirming the accuracy of the fits. While the O_1, O_2 origins have close to zero ISC yields, the yield for the dimer state R_5 is 63%, R_4 is 37%, and R_3 is $< 10\%$. (The present experimental configuration, which does not permit time delays of > 36 ns, is responsible for the uncertainty in the R_3 yield.) The key point of the dimer stimulated echo data is that *dimers composed of various configurations of monomer pairs have very different ISC rate constants, and in the system studied here, ISC is orders of magnitude faster for a dimer than for the corresponding monomers.*

Three distinct mechanisms could explain the differences in ISC for the various dimer states and the differences between the dimers and the corresponding O_1, O_2 monomers. The first mechanism involves a mechanical distortion of the pentacene molecules. When two pentacene molecules reside on adjacent lattice sites, there could be sufficient crowding in the lattice to result in a distortion of the pentacenes away from planarity. Normally, SOC between S_1 and T_1 is symmetry forbidden for $\pi\pi^*$ states of planar aromatic hydrocarbons. A mechanical distortion resulting in a reduction in pentacene symmetry can increase S_1–T_1 SOC and therefore ISC. This mechanism is improbable. The atom–atom potential calculations [19] indicate almost no crowding in the lattice. Therefore it is highly unlikely that pentacene is distorted at all, and any distortion that does occur will be very small. A small distortion can take matrix elements (two-center terms) which were strictly zero by symmetry and make them non-zero. However, these terms will still be close to zero and cannot account for the very large differences in ISC which are observed between monomer and dimer.

A second mechanism arises because of the delocalized nature of the dimer excited states. It has previously been shown that for delocalized exciton bands in molecular crystals, additional SOC terms are obtained if the finite overlap of nearest-

Table 2
Rate constants and ISC yields for pentacene dimers (all rate constants have been multiplied by 10^{-7})

Dimer	$1/\tau_f$	$2/T_2$	k_f^{SE}	k_{21}	k_{23}	ISC yield (β)
R_3	6.3 ± 0.5	6.0 ± 0.4	5.9 ± 0.1	–	–	< 0.1
R_4	7.9 ± 0.6	7.4 ± 0.2	7.4 ± 0.4	4.6 ± 0.4	2.7 ± 0.4	0.37 ± 0.05
R_5	13.5 ± 1.0	14.5 ± 0.4	14.1 ± 1.2	5.24 ± 0.4	8.8 ± 1.1	0.63 ± 0.04

neighbor molecular wavefunctions is accounted for [10]. These intermolecular SOC terms permit direct coupling between the T_1 and S_1 states due to the reduction in symmetry resulting from the extended nature of the exciton states and can cause significant ISC when the intramolecular SOC terms are symmetry forbidden. These results are directly applicable to delocalized dimer states. The rate of ISC due to this intermolecular SOC is proportional to the square of the overlap of the molecular wavefunctions. In this scenario, the dimers' ISC differs from the corresponding monomers' because of intermolecular SOC, and the dimers differ from each other because of differences in the overlap of the molecular wavefunctions for the various dimer configurations.

While the intermolecular SOC mechanism cannot be ruled out, it is not very plausible. Estimates of the size of the intermolecular SOC terms for a pair of benzene molecules arranged in a particular configuration [10], show that these terms are comparable in size to spin–orbit–vibronic terms which are normally responsible for ISC in $\pi\pi^*$ monomers. While this calculation is not for pentacene dimers, it suggests that intermolecular SOC will still result in a forbidden ISC process and therefore cannot account for the highly allowed ISC process displayed by the R_4 and R_5 dimers.

In the first two mechanisms considered above, it was assumed that there is no other triplet level, T_2, lying in the energy interval between T_1 and S_1. The third possible mechanism involves such a level. For the four pentacene origins, it was argued that large differences in ISC occur at 1.8 K because T_2 is accessible from S_1 excited states of O_3 and O_4 but inaccessible from the S_1 states of O_1 and O_2 [11].

A similar situation can occur for the dimers. As illustrated schematically in the inset of fig. 7, dimer formation results both in a splitting and level shift. The splitting is due to the dipole–dipole interaction between the pentacenes, while the shift arises from the changes in van der Waals interactions with the lattice in going from monomer to dimer, i.e. changes in the crystal shift [22]. The crystal shift in general will be different for singlet and triplet states, and there is no reason to assume that the change in crystal shift in going from monomer to dimer will be the same for singlet and triplet states. Since the second triplet state of the monomers O_1 and O_2 is only a few tens of cm^{-1} above the first singlet [11], it is not implausible that dimer formation can bring the dimer T_2 below the dimer S_1.

As with the monomers, this mechanism provides allowed SOC of S_1 to an accessible triplet state, and therefore very fast and efficient ISC. Since the level shifts will be somewhat different for the various dimer configurations, T_2 can be below S_1 for R_4 and R_5 resulting in allowed ISC, while T_2 is somewhat above S_1 for R_3 resulting in less efficient ISC. This third mechanism would appear to be the most likely. It invokes the same basic mechanism that is operative for the monomers. It provides a rationale for the dimers being vastly different from the corresponding O_1, O_2 monomers, for the dimer ISC being highly allowed, and for the various dimer ISC rate constants to differ significantly. Unfortunately, it is not possible to perform temperature-dependent fluorescence lifetime measurements on the dimers, which could provide evidence for this mechanism. At temperatures where a detectable decrease in fluorescence lifetime is expected, a large O_1, O_2 monomer hot-band absorption obscures the dimer fluorescence.

4. Concluding remarks

Using stimulated photon echoes, photon echoes, and fluorescence lifetime measurements we have examined the excited-state dynamics of the first singlet state of pentacene dimers and monomers in the *p*-terphenyl host crystal. At 1.8 K, the only contribution to the homogeneous linewidth is from lifetime broadening, i.e. there is no pure dephasing and $T_2 = 2\tau_t$. Stimulated echo measurements demonstrate that intersystem crossing from singlet delocalized dimer states to triplet dimer states can be orders of magnitude faster than intersystem crossing in the corresponding monomers. It was also quantitatively confirmed that the large differences in monomer lifetimes found for the four sites of pentacene in *p*-terphenyl are due solely to differences in intersystem crossing.

While several mechanisms were considered, the

mechanism deemed mostly likely to account for the large increase in dimer intersystem crossing over the corresponding monomers, involves a second triplet state close in energy to the first singlet state. Dimer formation shifts this second triplet below the dimer first singlet, opening an allowed intersystem crossing pathway for the dimers which does not exist for the monomers. While in some sense pentacene may be a special case because of the close proximity of the second triplet to the first singlet, the results presented here demonstrate that estimates of intersystem crossing in dimers cannot necessarily be made from information on intersystem crossing in the corresponding monomers.

Acknowledgement

This work was supported by the National Science Foundation, Division of Materials Research (DMR 80-20248). WLW would like to thank Bell Laboratories for a Cooperative Research Fellowship. MDF acknowledges the Simon Guggenheim Memorial Foundation for Fellowship support that contributed to this research.

References

[1] M.Y. Okamura, G. Feher and N. Nelson, Photosynthesis, Vol.1, ed. Govindjee (Academic Press, New York, 1982) ch. 5.

[2] R.W. Olson, F.G. Patterson, H.W.H. Lee and M.D. Fayer, Chem. Phys. Letters 79 (1981) 403;
H.W.H. Lee, F.G. Patterson, R.W. Olson, D.A. Wiersma and M.D. Fayer, Chem. Phys. Letters 90 (1982) 172;
H.W.H. Lee, F.G. Patterson, W.L. Wilson and M.D. Fayer, J. Chem. Phys., to be published.

[3] A.H. Zewail and C.B. Harris, Chem. Phys. Letters 28 (1974) 8;
A.H. Zewail and C.B. Harris, Phys. Rev. B11 (1975) 952;
W.G. Breiland, T.E. Altman and J.S. Voris, Chem. Phys. Letters 67 (1979) 30.

[4] B.J. Botter, A.J. van Strien and J. Schmidt, Chem. Phys. Letters 49 (1977) 39.

[5] J.B.W. Morsink and D.A. Wiersma, Chem. Phys. Letters 89 (1982) 291.

[6] J.L. Baudour, Y. Delugeard and H. Cailleau, Acta Cryst. B32 (1976) 150.

[7] R.W. Olson and M.D. Fayer, J. Phys. Chem. 84 (1980) 2001.

[8] S.K. Lower and M.A. El-Sayed, Chem. Rev. 66 (1966) 199.

[9] M.A. El-Sayed and J. Olmsted III, Chem. Phys. Letters 11 (1971) 568;
A.H. Francis and C.B. Harris, J. Chem. Phys. 57 (1972) 1050;
D.A. Antheunis, J. Schmidt and J.H. van der Waals, Chem. Phys. Letters 6 (1970) 255.

[10] D.E. Cooper and M.D. Fayer, J. Chem. Phys. 68 (1978) 229, and references therein.

[11] J.O. Williams, A.C. Jones and M.J. Davies, Proceedings of the Tenth Molecular Crystal Symposium, St. Jovite, Quebec, Canada (September 20–24, 1982) p. 303.

[12] J.B.W. Morsink, W.H. Hesselink and D.A. Wiersma, Chem. Phys. 71 (1982) 289.

[13] W.B. Mims, Electron paramagnetic resonance, ed. S. Geschwind (Plenum Press, New York, 1972) ch. 4;
P. Hu and S.R. Hartmann, Phys. Rev. B9 (1974) 1;
J.P. Klauder and P.W. Anderson, Phys. Rev. 125 (1962) 912.

[14] H. de Vries and D.A. Wiersma, J. Chem. Phys. 70 (1979) 5807.

[15] T.E. Orlowski and A.H. Zewail, J. Chem. Phys. 70 (1979) 1390.

[16] D.E. Cooper, R.D. Wieting, R.W. Olson and M.D. Fayer, Chem. Phys. Letters 67 (1979) 41.

[17] R.W. Olson, H.W.H. Lee, F.G. Patterson and M.D. Fayer, J. Chem. Phys. 76 (1982) 31.

[18] J.H. Meyling and D.A. Wiersma, Chem. Phys. Letters 20 (1973) 383.

[19] R.N. Lindsay and B.R. Markey, unpublished results.

[20] D.E. Cooper, R.W. Olson and M.D. Fayer, J. Chem. Phys. 72 (1980) 2332.

[21] P.R. Bevington, Data reduction and error analysis for the physical sciences (McGraw-Hill, New York, 1969) pp. 212–213.

[22] A.S. Davydov, Theory of molecular excitations (Plenum Press, New York, 1971).